**Journal of**

**Applied and Computational Mechanics**

Shahid Chamran
University of Ahvaz

Journal of *Applied and Computational Mechanics*

**Research Paper**

# Dynamic Response of Functionally Graded Carbon Nanotube-Reinforced Hybrid Composite Plates

## Chun-Sheng Chen[1] , Chin-Ping Fung[2] , Hai Wang[3] , Wei-Ren Chen[4]

[1] Department of Mechanical Engineering, Lunghwa University of Science and Technology, Guishan Shiang 33306, Taiwan, Email: cschenme@yahoo.com.tw

[2] Department of Mechanical Engineering, Oriental Institute of Technology, Pan-Chiao 22061, Taiwan, Email: cpfung@mail.oit.edu.tw

[3] Department of Mechanical Engineering, Ming Chi University of Technology, Tai-Shan 24301, Taiwan, Email: whai@mail.mcut.edu.tw

[4] Department of Mechanical Engineering, Chinese Culture University, Taipei 11114, Taiwan, Email: wrchen@ulive.pccu.edu.tw

**Abstract.** Dynamic instability behavior of functionally graded carbon nanotube reinforced hybrid composite plates subjected to periodic loadings is studied. The governing equations of motion of Mathieu-type are established by using the Galerkin method with reduced eigenfunctions transforms. With the Mathieu equations, the dynamic instability regions of hybrid nanocomposite plates are determined by using the Bolotin's method. Results reveal that the dynamic instability is significantly affected by the carbon nanotube volume fraction, layer thickness ratio, bending stress, static and dynamic load parameters. The effects of important parameters on the instability region and dynamic instability index of hybrid nanocomposite plates are discussed.

**Keywords:** Functionally graded; Volume fraction; Dynamic instability regions; Dynamic instability index.

## 1. Introduction

Composite plates can offer higher stiffness to weight ratio than traditional metal plates and have been used successfully in various engineering industries. When the composite plate is subjected to periodic in-plane loads, dynamic instability may occur due to parametric resonance. It has important theoretical and practical significance to accurately determine the dynamic stability area of the composite plate structure in the design stage [1, 2]. Sofiyev and his coworkers discussed in detail the dynamic instability of functionally graded cylindrical shells [3-5] and conical shells [6-8] under static and time-dependent periodic loads. First, the governing partial differential equations of cylindrical and conical shells with functionally graded interlayer were derived. Then the above governing equations were simplified to Mathieu-Hill differential equation describing dynamic instability, and the Bolotin's method was used to solve the excitation frequencies of cylindrical shells and truncated cone shells in order to understand the effects of the volume fraction index, shell characteristics, static and dynamic load factor on the unstable regions. In most cases, the mechanical properties of composite materials are enhanced by adding a high percentage of fibers to the matrix. Additionally, the tensile strength and elastic modulus of nanocomposites can be improved by adding a small amount of nanotubes to the matrix. The performance of the composite plate reinforced with a small percentage of nanotubes is even better than that of the composite plate using conventional carbon fibers. Therefore, many publications [9-13] have focused on the vibration and stability of functionally graded carbon nanotube (CNT) reinforced composite plates.

Based on the Euler and Timoshenko beam theories, the dynamic stability of embedded single-walled CNTs beam under axial compression was studied by Ansari *et al.* [14]. A Winkler-type elastic foundation was employed to represent the interaction of the CNT and the surrounding elastic medium. The influences of the static load factor, temperature change, slenderness ratio and spring constant of the elastic medium on the dynamic stability characteristics of the nanocomposite beam were presented. Yas and Heshmati [15] investigated the vibrational properties of nanocomposite beams reinforced by randomly oriented straight CNTs under moving load. An embedded carbon nanotube in a polymer matrix and its surrounding inter-phase was replaced with an equivalent fiber for predicting the mechanical properties of the carbon nanotube/polymer composite. The Newmark method was also used to evaluate the time response of the system. The effects of material distribution, CNT orientation, moving load velocity, slenderness ratio and boundary conditions on the dynamic characteristics of nanocomposite beams were showed. Bhardwaj *et al.* [16] presented the nonlinear flexural and dynamic responses of CNT reinforced laminated composite plates. The CNT-reinforced polymer matrix was treated as new matrix and then reinforced with glass fiber in an orthotropic manner. The effects of the percentage of CNT and aspect ratio on the dynamic response of the nanocomposite plates were presented.

The dynamic analysis of nanocomposite cylinders reinforced by CNTs subjected to impact loads was presented by Rasool *et al.* [17]. Four types of distribution of arranged CNTs are considered; uniform distribution and three functionally graded distributions

along the radial direction of the cylinder. The effects of the distribution type and volume fraction of CNTs on the frequency and stress wave propagation of CNT-reinforced cylinders were investigated. Ke and Yang [18] presented the dynamic stability of functionally graded nanocomposite beams reinforced by CNTs based on Timoshenko beam theory. The boundary of unstable region was determined by the Bolotin's method. A parametric study was conducted to study the influence of CNT volume fraction and slenderness ratio on the dynamic stability characteristics of nanocomposite beams. Rafiee et al. [19] studied the nonlinear dynamic stability of piezoelectric functionally graded CNT-reinforced composite plates under external resonance. The governing equations of the piezoelectric nanocomposite plates were derived based on the first-order plate theory and von Kármán hypothesis. It was assumed that the single-walled CNTs were aligned, straight and uniformly laid out. The periodic solution and its stability were determined by using the harmonic balance method. The effect of the applied voltage, defect, volume fraction and distribution pattern of nanocomposite plates on the parametric resonance was investigated.

The dynamic stability of CNT-reinforced functionally graded cylindrical panels and plates under static and periodic axial forces were presented by Lei et al. [20, 21]. The cylindrical plates were reinforced by single-walled CNTs with uniform and functionally graded distributions of CNTs along the plate thickness direction. The extended rule of mixture was employed to estimate the effective material properties of the resulting nanocomposites. The principal instability regions were analyzed by Bolotin's first-order approximation. The influences of CNTs volume fraction, aspect ratio and distribution type on the dynamic instability were examined. A new and improved plate model was presented for the vibration characteristics of functionally graded plates by Belkorissat et al. [22]. The displacement field of this theory was chosen based on the hyperbolic variation of the in-plane displacements. The effects of plate thickness, aspect ratio, and various material compositions on the dynamic response of functionally graded nanocomposite plates were studied. Wang and Shen [23] investigated the dynamic response of CNT-reinforced composite plates resting on elastic foundations. A single-layer nanocomposite plate and a three-layer plate composed of a homogeneous core and two CNT-reinforced composite sheets were considered. The CNT reinforcement was either uniformly distributed or functionally graded in the thickness direction. The effects of volume fraction distribution, foundation stiffness, initial stress, and the core-to-face thickness ratio on the dynamic behavior of nanocomposite plates were discussed. The impact behavior of hybrid glass-carbon composite plates was investigated by Sayer et al. [24]. The energy profiling method was used together with the load–deflection curve to determine the thresholds of hybrid composites. The failure process of the damaged specimen was evaluated by comparing the load–deflection curve with the image of the damaged sample. The nonlinear dynamic instability analysis of FG CNT-reinforced composite plates resting on elastic foundations was investigated by Fu et al. [25] using the classic plate theory. Based on the two-step perturbation technique, a Mathieu-type equation was formulated, and the effect of various factors on the dynamic unstable zones was studied by using the method of incremental harmonic balance. Wu et al. [26] investigated the dynamic instability of FG graphene-reinforced nanocomposite plates based on the differential quadrature method combined with the Bolotin's method. The system equations were established using the first-order plate theory. Numerical results showed that adding a small amount of graphene platelet would enlarge the natural frequency, but would decrease the instability region. Singh et al. [27] presented a semi-analytical approach to study the dynamic instability of FG CNT-reinforced composite plates under uniform and non-uniform in-plane loads. Based on the Hamilton's principle, the governing equations were derived, and transformed into Mathieu type equations by the Galerkin's method. Then, the Bolotin's method was applied to solve Mathieu type equations to determine the unstable boundaries.

The active vibration of hybrid composite and fiber multilayered plates integrated with piezoelectric fiber reinforced composite sensors and actuators was studied by Kapuria et al. [28]. The effective electromechanical properties of the piezoelectric fiber reinforced laminas were computed using a coupled iso-field micromechanical model. The effects of piezoelectric fiber orientation, volume fraction and dielectric ratio on the control response were investigated. Khalili and Yasin [29] presented the dynamic analysis of sandwich beams with shape memory alloy hybrid composite face sheets and flexible core. The influence of the shape memory alloy wires vibration phenomena and thickness location inside the composite face sheets and the dynamic response were analyzed. The dynamic analysis of functionally graded CNTs-reinforced composite structures was studied by Frikh et al. [30]. Zero transverse shear stress was applied to the top and bottom surfaces. Four types of distributions of CNTs were considered, namely uniform distribution and three functionally gradient distributions. The extended rule of mixture was used to estimate the effective material properties of the CNT-reinforced composite plate. The effects of volume fractions, profiles of CNTs and geometrical parameters on dynamic behaviors of functionally graded CNTs reinforced plates were presented.

It is worth noting that the hybrid fiber-reinforced metal laminate composite plates made of a fiber reinforced polymer core covered by face-sheet metal have higher wear and corrosion resistance than traditional composite plates [31]. Thus, when designing a plate structure in a thermal environment, a hybrid nanocomposite plate with face-sheet metal is a good choice. In these previous studies, the investigation concerning the sandwich plate with metal face sheets subjected to an arbitrary dynamic load has seldom been reported. The dynamic vibration of hybrid composite plates was analyzed previously by the first author and coworkers [32, 33]. However, there is no literature to study the dynamic behavior of hybrid nanocomposite plates under arbitrary periodic loads. In the present study, the dynamic stability behavior of a three-layer hybrid nanocomposite plate under arbitrary dynamic loads is studied. Three kinds of CNT-reinforced hybrid nanocomposite plate are considered, in which the single-walled CNTs in the core layer are assumed to be uniformly distributed (FG-U) or symmetric functionally graded (FG-X and FG-O). The Galerkin method is applied to the governing partial differential equations to yield ordinary differential equations. Then, the Mathieu-type equations are formed and solved by employing Bolotin's method to determine the regions of dynamic instability of hybrid nanocomposite plates. The effects of CNT volume fraction, distribution type, layer thickness ratio, static and dynamic load parameter on the dynamic instability boundary and dynamic instability index of hybrid nanocomposite plates are investigated and discussed.

## 2. Modeling of nanocomposite plate

Following the similar technique described by Chen et al. [34], the perturbation method is used to derive the system equations of motion of the CNTs-reinforced hybrid nanocomposite plate under dynamic load, including the effects of rotary inertia and transverse shear. The governing equation is expressed as

$$(\sigma_{ij}\bar{u}_{s,j})_{,i} + [\bar{\sigma}_{ij}(\delta_{sj} + u_{s,j} + \bar{u}_{s,j})]_{,i} + F_s + \Delta F_s = \rho\ddot{\bar{u}}_s \tag{1}$$

where $\sigma_{ij}$, $\bar{\sigma}_{ij}$, $\bar{F}_s$ and $\Delta F_s$ are the initial stress, perturbing stress, body force and perturbed body force, respectively. $u_s$, $\bar{u}_s$ and $\rho\ddot{\bar{u}}_s$ represent the initial displacement, incremental displacement and inertia force and $\rho$ is the mass density.

In order to account for the transverse shear deformation and rotary inertia effects in a nanocomposite plate, the displacements assumes the following forms based on Mindlin plate theory:

$$u(x,y,z,t)=u_x(x,y,t)+z\phi_x(x,y,t)$$

$$v(x,y,z,t)=v_y(x,y,t)+z\phi_y(x,y,t)$$

$$w(x,y,z,t)=w_z(x,y,t) \tag{2}$$

where $u_x$, $v_y$ and $w_z$ are displacements at the midplane in the respective x, y and z direction; $\phi_x$ and $\phi_y$ are rotation angles about y and x axes, respectively. The x and y axes of the coordinate system are set to coincide with the two edges of the rectangular nanocomposite plate. The constitutive matrix equation of the nanocomposite plate is given by:

$$
\begin{bmatrix} \sigma_{xx} \\ \sigma_{yy} \\ \sigma_{yz} \\ \sigma_{zx} \\ \sigma_{xy} \end{bmatrix} =
\begin{bmatrix} C_{11} & C_{12} & 0 & 0 & C_{16} \\ C_{12} & C_{22} & 0 & 0 & C_{26} \\ 0 & 0 & C_{44} & C_{45} & 0 \\ 0 & 0 & C_{45} & C_{55} & 0 \\ C_{16} & C_{26} & 0 & 0 & C_{66} \end{bmatrix}
\begin{bmatrix} \varepsilon_{xx} \\ \varepsilon_{yy} \\ \varepsilon_{yz} \\ \varepsilon_{zx} \\ \varepsilon_{xy} \end{bmatrix} \tag{3}
$$

The plate is subjected to an arbitrary periodic stress system that changes with time, and the states of the periodic load is a combination of pulsating compressive stress $\sigma_{ij}^n$ and pure pulsating bending stress $\sigma_{ij}^m$. The periodic initial load system is assumed to have the form:

$$\sigma_{ij}=\sigma_{ij}^n + 2z\sigma_{ij}^m / h = (\sigma_{ij}^S + \sigma_{ij}^D \cos\varpi t) + 2z(\sigma_{ij}^{Sm} + \sigma_{ij}^{Dm}\cos\varpi t)/h \quad (\text{ i, j = x, y, z }) \tag{4}$$

which consists of the spatially uniform longitudinal, transverse, shear, bending and twisting stresses. Here $\sigma_{ij}^S$ and $\sigma_{ij}^D$ are the static and dynamic components of the periodic normal or shear stress $\sigma_{ij}^n$; $\sigma_{ij}^{Sm}$ and $\sigma_{ij}^{Dm}$ are the static and dynamic components of the periodic pure bending or torsion stress $\sigma_{ij}^m$; $\varpi$ is the angular frequency of external excitation. Substitute the displacement field (2), Eqs. (3) and (4) into Eq. (1), and then integrate them. The dynamic motion equations of nanocomposite plate can be written as

$$
\begin{aligned}
&[ A_{11} u_{x,x} + A_{16} ( u_{x,y} + u_{y,x})+ A_{12}\ u_{y,y} + B_{11}\ \phi_{x,x} + B_{16} ( \phi_{x,y} + \phi_{y,x})+ B_{12}\ \phi_{y,y} + N_{xx}u_{x,x} + M_{xx}\phi_{x,x} + N_{xy}u_{x,y} + M_{xy}\phi_{x,y} + N_{xz}u_{z,x} ]_{,x} +[ A_{16}\ u_{x,x} \\
&+ A_{26}\ u_{y,y} + A_{66} ( u_{x,y}+u_{y,x})+ B_{16}\ \phi_{x,x} + B_{66} ( \phi_{x,y}+\phi_{y,x})+ B_{26}\ \phi_{y,y} + N_{yy}u_{x,y} + M_{yy}\phi_{x,y} + N_{xy}u_{x,x} + M_{xy}\phi_{x,x} + N_{yz}u_{z,x} ]_{,y} + f_x = \rho h \ddot{u}_x
\end{aligned} \tag{5}
$$

$$
\begin{aligned}
&[ A_{16}\ u_{x,x} + A_{66} ( u_{x,y}+u_{y,x} )+ A_{26}\ u_{y,y} + B_{16}\ \phi_{x,x} + B_{66} ( \phi_{x,y}+\phi_{y,x} )+ B_{26}\ \phi_{y,y} + N_{xx}u_{y,x} + M_{xx}\phi_{y,x} + N_{xy}u_{y,y} + M_{xy}\phi_{y,y} + N_{xz}u_{z,y} ]_{,x} \\
&+[ A_{12}\ u_{x,x} + A_{26} ( u_{x,y}+u_{y,x} )+ A_{22}\ u_{y,y} + B_{12}\ \phi_{x,x} + B_{26} ( \phi_{x,y}+\phi_{y,x} )+ B_{22}\ \phi_{y,y} \\
&+ N_{yy}u_{y,y} + M_{yy}\phi_{y,y} + N_{xy}u_{y,x} + M_{xy}\phi_{y,x} + N_{yz}u_{z,y} ]_{,y} + f_y = \rho h \ddot{u}_y
\end{aligned} \tag{6}
$$

$$[ A_{55} ( w_{,x}+\phi_x )+ A_{45} ( w_{,y}+\phi_y )+ N_{xx}w_{,x} +N_{xy}w_{,y} ]_{,x} +[ A_{45} ( w_{,x}+\phi_x )+ A_{44} ( w_{,y}+\phi_y )+ N_{xy}w_{,x} + N_{yy}w_{,y} ]_{,y} + f_z = \rho h \ddot{w} \tag{7}$$

$$
\begin{aligned}
&[ B_{11}u_{x,x} + B_{16} ( u_{x,y} + u_{y,x} )+ B_{12}\ \phi_{y,y} + D_{11}\phi_{x,x} + D_{16} ( \phi_{x,y} +\phi_{y,x} )+ D_{12}\ \phi_{y,y} + M_{xx}u_{x,x} + M_{xx}^*\phi_{x,x} + M_{xy}u_{x,y} + M_{xy}^*\phi_{x,y} + M_{xz}u_{z,x} ]_{,x} \\
&+[ B_{16}\ u_{x,x} + B_{66} ( u_{x,y}+u_{y,x} )+ B_{26}\ u_{y,y} + D_{16}\ \phi_{x,x} + D_{66} ( \phi_{x,y}+\phi_{y,x} )+ D_{26}\ \phi_{y,y} + M_{xx}u_{x,y} + M_{yy}^*\phi_{x,y} + M_{xy}u_{x,x} + M_{xy}^*\phi_{x,x} + M_{yz}u_{z,x} ]_{,y} \\
&- A_{55} ( w_{,x}+\phi_x )- A_{45} ( w_{,y}+\phi_y )-( N_{xz}u_{x,x} + M_{xz}\phi_{x,x} + N_{zz}\phi_x + N_{zy}u_{x,y} + M_{zy}\phi_{x,y} )+ m_x = \rho h^3 \ddot{\phi}_x / 12
\end{aligned} \tag{8}
$$

$$
\begin{aligned}
&[ B_{16}\ u_{x,x} + B_{66} ( u_{x,y}+u_{y,x} )+ B_{26}\ u_{y,y} + D_{16}\ \phi_{x,x} + D_{66} ( \phi_{x,y}+\phi_{y,x} )+ D_{26}\ \phi_{y,y} + M_{xx}u_{y,y} + M_{xx}^*\phi_{y,x} + M_{xy}u_{y,y} + M_{xy}^*\phi_{y,y} + M_{xz}u_{z,y} ]_{,x} \\
&+[ B_{26} ( u_{x,y}+u_{y,x} )+ B_{12}u_{x,x} + B_{22}\ u_{y,y} + D_{12}\ \phi_{x,x} + D_{26} ( \phi_{x,y}+\phi_{y,x} )+ D_{22}\ \phi_{y,y} + M_{yy}u_{y,y} + M_{yy}^*\phi_{y,y} + M_{xy}u_{y,x} + M_{xy}^*\phi_{y,x} + M_{xz}u_{z,y} ]_{,y} \\
&- A_{45} ( w_{,x}+\phi_x )- A_{44} ( w_{,y}+\phi_y )-( N_{xz}u_{y,x} + M_{xz}\phi_{y,x} + N_{zz}\phi_{yx} + N_{zy}u_{y,y} + M_{zy}\phi_{y,y} )+ m_y = \rho h^3 \ddot{\phi}_y / 12
\end{aligned} \tag{9}
$$

where

$$( A_{ij},B_{ij},D_{ij} ) = \int C_{ij} ( 1,z,z^2 ) \, dz \quad ( i, j = 1, 2, 6 )$$

$$( A_{ij},B_{ij},D_{ij} ) = \int \kappa \, C_{ij} ( 1,z,z^2 ) \, dz \quad ( i, j = 4, 5)$$

$$( N_{ij},M_{ij},M_{ij}^* ) = \int \sigma_{ij} ( 1,z,z^2 ) \, dz \quad ( i, j = x, y, z ) \tag{10}$$

Here $A_{ij}$, $B_{ij}$ and $D_{ij}$ are the stiffness coefficients; $N_{ij}$, $M_{ij}$ and $M_{ij}^*$ are the arbitrary load resultants. $C_{ij}$'s are the elastic constants and $\kappa$ is the shear correction factor. $f_x$, $f_y$, $f_z$, $m_x$ and $m_y$ are the lateral loadings. All integrations are done through the plate thickness from -h/2 to h/2.

In order to simulate the influence of CNTs on the core layer, the extended rules of mixture micromechanical model are used to evaluate the effective Young's modulus and shear modulus:

$$E_{11} = \eta_1 V_{CN}E_{11}^{CN} + V_M E^M \tag{11}$$

$$\frac{\eta_2}{E_{22}} = \frac{V_{CN}}{E_{22}^{CN}} + \frac{V_M}{E^M}$$

$$\frac{\eta_3}{G_{12}} = \frac{V_{CN}}{G_{12}^{CN}} + \frac{V_M}{G^M}$$

where $V_{CN}$ and $V_M$ are the volume fractions of the CNTs and the matrix of nanocomposite plate, respectively. $E_{11}^{CN}$, $E_{22}^{CN}$ and $G_{12}^{CN}$ are Young's and shear modules of the CNTs; $E_M$ and $G_M$ are Young's and shear modules of the matrix; $\eta_1$, $\eta_2$ and $\eta_3$ are the CNT efficiency parameters. The size-dependent CNT efficiency parameters can be obtained from the rule of mixture. It is assumed that the single-walled CNT reinforced material of the core layer of the studied hybrid nanocomposite plate has uniform (FG-U) or symmetric functionally graded (FG-X, FG-O) distributions. For symmetric-type nanocomposite plates, the volume fraction $V_{CN}$ of CNTs is assumed as:

$$\text{FG-O}: \quad V_{CN}(z) = 2(1 - \frac{2|z|}{h})V_{CN}^* \tag{12}$$

$$\text{FG-X}: \quad V_{CN}(z) = 4(\frac{|z|}{h})V_{CN}^* \tag{13}$$

where $V_{CN}^* = w_{CN} / (w_{CN} + (\rho_{CN} / \rho_M)(1 - w_{CN}))$. $w_{CN}$ is the mass fraction of CNTs. $\rho_{CN}$ and $\rho_M$ are the respective CNTs and matrix mass densities, and are related to the mass density of the core layer by

$$\rho = V_{CN}\rho_{CN} + V_M\rho_M \tag{14}$$

and

$$V_{CN} + V_M = 1 \tag{15}$$

## 3. Dynamic instability analyses

The hybrid nanocomposite plate investigated in this study consists of three layers. The top and bottom layers are made of a metal and the material of the middle layer is a functionally graded CNTs-reinforced composite. The configuration of functionally graded CNTs-reinforced hybrid nanocomposite plate is shown in Fig. 1. In the core layer of the hybrid nanocomposite plate, the matrix is isotropic and the CNTs are uniformly distributed or functionally graded along the thickness direction. The CNTs are assumed to be aligned and straight with a uniform layout. Different distribution profiles of CNTs are shown in Fig. 2. FG-U stands for a uniformly distributed CNTs layer. FG-X and FG-O represent two symmetric distributions of the volume fraction of CNTs in the functionally graded CNTs-reinforced composite layer.

Since arbitrary periodic loads in the governing equations (5)-(9) of the hybrid nanocomposite plate will lead to very complicated conditions, it is difficult to discuss the results of all cases. Therefore, the object to be investigated in this study is the dynamics of a simply supported hybrid nanocomposite plate subjected to a periodic load system, which is composed of pulsating longitudinal normal stress and pulsating pure bending stress. Assuming that all other stresses are zero, the stress system equation (4) is simplified to

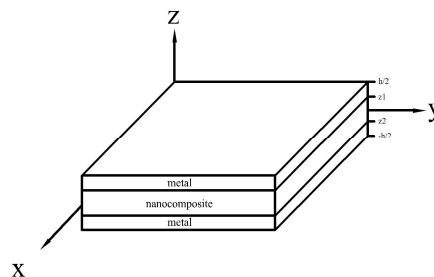$$\sigma_{xx} = \sigma_n + 2z\sigma_m / h \tag{16}$$



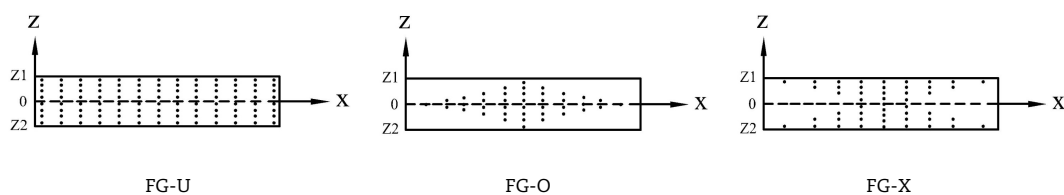**Fig. 1.** The functionally graded CNTs reinforced composite plate



**Fig. 2.** Different CNTs distributions profiles

where $\sigma_n = \sigma_{xx}^S + \sigma_{xx}^D \cos \varpi t = \sigma^S + \sigma^D \cos \varpi t$ and $\sigma_m = \sigma_{xx}^{Sm} + \sigma_{xx}^{Dm} \cos \varpi t = \sigma^{Sm} + \sigma^{Dm} \cos \varpi t$. $\sigma^S$, $\sigma^D$, $\sigma^{Sm}$ and $\sigma^{Dm}$ are the static and dynamic stress components. The only nonzero periodic loads are $N_{xx} = h\sigma_n$, $M_{xx} = Sh^2\sigma_n / 6$, $M_{xx}^* = h^3\sigma_n / 12$, where bending ratio $S = \sigma_m / \sigma_n$ is the ratio of bending stress to normal stress. When S=0, there exists no initial bending stress. The lateral loads and body forces $f_x$, $f_y$, $f_z$, $m_x$ and $m_y$ are taken to be zero. The hybrid nanocomposite plate has boundary edges along x=0 and a, y=0 and b, all of which are simply supported. Based on the Navier solution procedure, the displacement fields satisfying the above geometric boundary conditions can be given as follows

$$u_x = \sum\sum h\, U_{mn}(t) \cos(m\pi x/a) \sin(n\pi y/b)$$

$$u_y = \sum\sum h\, V_{mn}(t) \sin(m\pi x/a) \cos(n\pi y/b)$$

$$w = \sum\sum h\, W_{mn}(t) \sin(m\pi x/a) \sin(n\pi y/b) \tag{17}$$

$$\phi_x = \sum\sum \Psi_{xmn}(t) \cos(m\pi x/a) \sin(n\pi y/b)$$

$$\phi_y = \sum\sum \Psi_{ymn}(t) \sin(m\pi x/a) \cos(n\pi y/b)$$

Assume that the displacement parameters $[U_{mn}, V_{mn}, W_{mn}, \Psi_{xmn}, \Psi_{ymn}]^T$ can be expressed as $\Delta(t) = \overline{\Delta} f(t)$. $\Delta(t)$ and $\overline{\Delta}$ denote the time dependent and time independent displacement vector, respectively. Substituting Eq. (17) into governing equations (5)-(9) and applying the Galerkin method leads to the governing matrix equation of motion

$$\{([K]+[G])\, f(t) + [M]\, (d^2\, f(t)/dt)\}\overline{\Delta} = 0 \tag{18}$$

where [K], [G] and [M] are the elastic stiffness matrix, geometric stiffness matrix and consistent mass matrix, respectively. Equation (18) represents the following three eigenvalue problems: (i) free vibration, (ii) static buckling stability and (iii) dynamic instability.

To study the buckling of the hybrid nanocomposite plate, by neglecting the consistent mass term [M] in Eq. (18) and setting f(t)=1, the eigenvalue equation for the static buckling loads $N_{xx}$ is expressed as follows

$$\{[K]-(N_{xx})[G]\}\overline{\Delta} = 0 \tag{19}$$

By setting [G]=0 and $f(t) = e^{i\omega t}$, the eigenvalue equation of free vibration is obtained from Eq. (18) as

$$\{[K] - \omega^2\, [M]\}\overline{\Delta} = 0 \tag{20}$$

which will be used to analyze the free vibration of the hybrid nanocomposite plate. The condition for the existence of the nontrivial solutions is that the determinant of coefficients should vanish. Hence, the natural frequency $\omega_n$ can be obtained from the equation

$$\left\| [K] - \omega_n^2 [M] \right\| = 0 \tag{21}$$

The non-zero periodic load in Eq. (16) for the dynamic stability analysis of the hybrid nanocomposite plate can be written as

$$N_{xx} = -(\alpha_S\, P_{cr} + \alpha_D\, P_{cr}\, \cos \varpi t) \tag{22}$$

where $\alpha_S = h\,\sigma^S / P_{cr}$, $\alpha_D = h\,\sigma^D / P_{cr}$. $P_{cr}$ is the buckling load of the hybrid nanocomposite plate. $\alpha_S$ and $\alpha_D$ are the static and dynamic load parameters, respectively. Substituting Eq. (22) into Eq. (18) gives

$$\{([K]+(\alpha_S)\, P_{cr}\, [G]+(\alpha_D)\, P_{cr}\, [G] \cos \varpi t)\, f(t) + [M](d^2\, f(t)/dt)\}\overline{\Delta} = 0 \tag{23}$$

Equation (23) expresses the dynamic stability of the hybrid nanocomposite plate under periodic in-plane loads. To determine the instability regions, the Bolotin's method is used to obtain the dynamic instability boundary. Here the periodic solutions with period 2T and T are represented by Fourier series as

$$f(t)\,\overline{\Delta} = \sum_{k=1,3,5\ldots}^{\infty} \left(a_k \sin\frac{k\varpi t}{2} + b_k \cos\frac{k\varpi t}{2}\right) \tag{24}$$

$$f(t)\,\overline{\Delta} = \sum_{k=0,2,4\ldots}^{\infty} \left(a_k \sin\frac{k\varpi t}{2} + b_k \cos\frac{k\varpi t}{2}\right) \tag{25}$$

where $a_k$ and $b_k$ are arbitrary time invariant constants. By substituting the Fourier series solutions (24) and (25) into Eq. (23) and separating sine and cosine parts, two sets of linear algebraic equations in $a_k$ and $b_k$ are obtained for each solution. The eigenvalue system of the dynamic stability boundaries with period 2T is given as

$$\begin{vmatrix} [K] + \alpha_S P_{cr}[G] \pm \frac{1}{2}\alpha_D P_{cr}[G] - \frac{1}{4}\varpi^2[M] & \frac{1}{2}\alpha_D P_{cr}[G] & \ldots \\ \frac{1}{2}\alpha_D P_{cr}[G] & [K] + \alpha_S P_{cr}[G] - \frac{9}{4}\varpi^2[M] & \ldots \\ \ldots & \ldots & \ldots \end{vmatrix} = 0 \tag{26}$$

For the period T, the eigenvalue systems are

$$
\begin{vmatrix}
[K] + \alpha_S P_{cr}[G] - \varpi^2[M] & \frac{1}{2}\alpha_D P_{cr}[G] & ..... \\
\frac{1}{2}\alpha_D P_{cr}[G] & [K] + \alpha_S P_{cr}[G] - 4\varpi^2[M] & ..... \\
... & ... & .....
\end{vmatrix} = 0
\tag{27}
$$

and

$$
\begin{vmatrix}
[K] + \alpha_S P_{cr}[G] & \alpha_D P_{cr}[G] & ..... \\
\alpha_D P_{cr}[G] & [K] + \alpha_S P_{cr}[G] - \varpi^2[M] & ..... \\
... & ... & .....
\end{vmatrix} = 0
\tag{28}
$$

The stability-instability boundary frequencies can be obtained from the determinants (26)-(28). The determinants are infinite, but the results can be determined by considering only the first few terms. The boundary of primary unstable zone with a period of 2T is usually much larger than that of the secondary unstable region with a period of T, so it is of greater importance in practical engineering. Since the first-order approximation ( $a_1$ and $b_1$ ) of the primary unstable region is capable of obtaining solutions with sufficient accuracy [35], the boundary of the primary instability zone of dynamic stability can be determined as [27]

$$
\left| [K] + \alpha_S P_{cr}[G] \pm \tfrac{1}{2}\alpha_D P_{cr}[G] - \tfrac{1}{4}\varpi^2[M] \right| = 0
\tag{29}
$$

## 4. Numerical results and discussions

In this study, the dynamic instability of a three-layer hybrid nanocomposite plates is investigated, which is composed of two aluminum laminates and a functionally graded CNT-reinforced composite layer. The top and bottom layers are aluminum, and the core layer of the hybrid composite plate is CNTs reinforced composite. The single-walled CNTs are assumed to be uniformly distributed (FG-U) or symmetrical functionally graded (FG-X and FG-O). The material properties of the functionally graded CNT-reinforced composite layer gradually change in the thickness direction, and are evaluated by a micromechanical model.

The middle layer of the hybrid plate is a CNT-reinforced nano-layer, and PMMA is selected as the matrix. The total thickness of the hybrid Al/nanolayer/Al plate is h; $h_1$, $h_2$ and $h_3$ are the individual layer thickness of Al, nanolayer and Al, respectively. The layer thickness ratio is defined as $\gamma = t_{CNT} / t_{Al} = h_2 / h_1 = h_2 / h_3$, $h_1 = h_3$, so an increase in the layer thickness ratio indicates an increase in the core layer thickness. For the case of $\gamma$ =0, the hybrid plate is a pure aluminum plate. On the other hand, when $\gamma$ is infinite, the hybrid plate is a pure nanocomposite plate. The material properties of Al and PMMA in the analysis are as follows [36, 37]:

Aluminum: E=72GPa, G=28Gpa, $\upsilon$ =0.33, $\rho$ =2780 $kg/m^3$     PMMA: $\upsilon_m$ =0.34, $\rho_m$ =1150 $kg/m^3$, $E_m$ =2.23 GPa,

The material properties of CNTs are assumed to be single-walled CNTs of the armchair (10, 10) type and are determined by molecular dynamic simulations [38, 39]. The Young's and shear modulus are $E_{11}^{CN}$ =5.6466TPa, $E_{22}^{CN}$ =7.0800TPa, $G_{12}^{CN}$ = 1.9445TPa, and the density is $\rho_{CNT}$ =1400 $kg/m^3$. The CNT efficiency parameters ( $\eta_1$, $\eta_2$, $\eta_3$ ) can be determined by matching the effective material properties of CNT obtained from the rule of mixture. The CNT efficiency parameters from the molecular dynamics simulations are given in Table 1 [37, 40]. These efficiency parameters alongside with $G_{12} = G_{13}$, $G_{23} = 1.2G_{13}$ will be used in all the following examples.

The following non-dimensional coefficients of excitation frequency $\Omega = \varpi b^2 \sqrt{\rho_M / h^2 E_M}$, instability region $\Delta\Omega = \Omega^U - \Omega^L$ and dynamic instability index $\Omega_{DI}$ =100 $\Delta\Omega /( \omega_{nf} \, K_{cr} )$ are defined and used to evaluate the dynamic stability of the hybrid nanocomposite plates. $\Omega^U$ and $\Omega^L$ are the upper and lower excitation frequency, respectively. $\omega_{nf}$ is the non-dimensional fundamental natural frequency given by $\omega_{nf} = \omega b^2 \sqrt{\rho_M / h^2 E_M}$ and $K_{cr}$ is the dimensionless critical buckling load denoted by $K_{cr} = N_{xx} b^2 / E_M h^4$. The dynamic instability index $\Omega_{DI}$ indicates the relationship between the unstable region, the natural frequency and the buckling load. The influence of various variables of the hybrid nanocomposite plate on its dynamic instability will be examined and discussed next. The accuracy of the presented model for the analysis of the dynamic behaviors of the hybrid plate was verified in the authors' earlier study [24]. To prove the accuracy of the proposed method for the nanocomposite plate, the natural frequencies and critical buckling loads for various single CNT reinforced composite square plates are presented and compared with those by other investigators in Tables 2 and 3. It can be observed that the presented results are in close agreement with those by Alibeigloo and Emtehani [41], Lei et al. [42] and Malekzadeh and Shojaee [43]. Through these comparisons, the reliability and accuracy of the present computer program is assured.

**Table 1.** The single walled CNTs efficiency parameters

| $V_{CN}^*$ | $\eta_1$ | $\eta_2$ | $\eta_3$ |
|---|---|---|---|
| 0.11 | 0.149 | 0.934 | 0.653 |
| 0.14 | 0.150 | 0.941 | 0.659 |
| 0.17 | 0.149 | 1.381 | 0.967 |
| 0.28 | 0.141 | 1.585 | 1.109 |

**Table 2.** Effects of CNT volume fraction and distribution on the natural frequency for CNT reinforced square plates (a/b =1, a/h=10)

| Type | Source | $V_{CN}^*$ | | |
|---|---|---|---|---|
| | | 0.11 | 0.14 | 0.17 |
| FG-U | A | 13.555 | 14.357 | 16.838 |
| | Present | 13.229 | 14.025 | 16.571 |
| FG-O | A | 11.332 | 12.125 | 14.103 |
| | Present | 11.368 | 12.195 | 14.183 |
| FG-X | A | 14.668 | 15.388 | 18.173 |
| | Present | 14.216 | 14.982 | 17.908 |

A: Comparative data by Alibeigloo and Emtehani [41]

**Table 3.** Effects of CNT distribution types on the critical buckling load for CNT reinforced square plates (a/b =1, a/h=10, $V_{CN}^*$ =0.11)

| Source | Type | | |
|---|---|---|---|
| | FG-U | FG-O | FG-X |
| B | 30.9076 | 17.7534 | 40.8005 |
| C | 31.5258 | 19.0745 | 41.7608 |
| Present | 31.4551 | 18.9875 | 41.6484 |

B: Comparative data by Lei et al. [42]
C: Comparative data by Malekzadeh and Shojaee [43]

Figures 3 and 4 present the effects of static and dynamic load parameters on the excitation frequency ratio $\Omega / \omega_{nf}$, respectively. It can be seen, the primary instability region appears near the position where $\Omega$ is equal to 2 $\omega_{nf}$, that is, $\Omega / \omega_{nf}$ =2. It is evident that the compressive static load ($\alpha_S$ >0) produces a softening effect on the excitation frequency ratio and reduces the instability region. On the other hand, the tensile static load ($\alpha_S$ <0) has a reverse effect. Hybrid nanocomposite plates with various layer thickness ratios, CNT volume fractions and CNT distribution types also have the same results. It is attributable to that the excitation frequency ratio is independent of CNT volume fraction and distribution type. Regardless of the compressive or tensile static load, the distance between the two boundaries increases with the static load parameter. The increase of the dynamic load parameter increases the upper excitation frequency ratio and decreases the lower excitation frequency ratio. The influence of dynamic load parameters on the excitation frequency ratio is more significant than that of static load parameters.
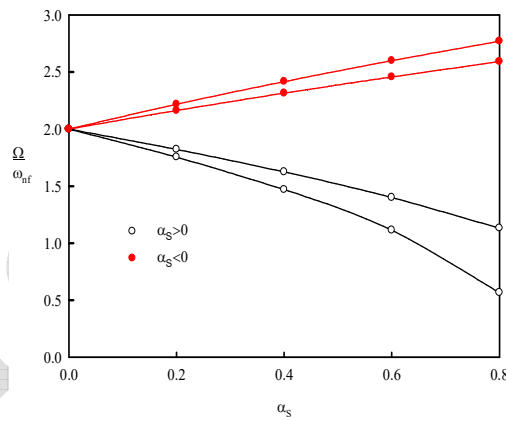


**Fig. 3.** Effect of static load types on excitation frequency ratio (a/b=1, a/h=10, $\alpha_D$/|$\alpha_S$|=0.3, S=0)
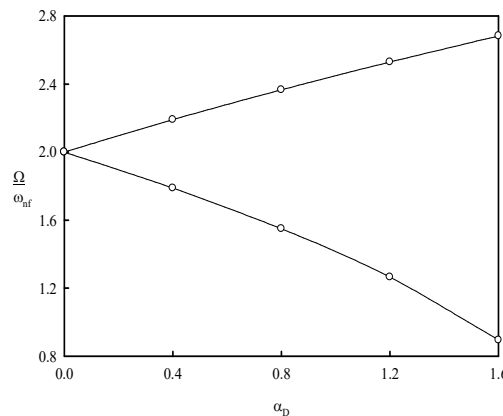


**Fig. 4.** Effect of dynamic load parameters on excitation frequency ratio (a/b=1, a/h=10, $\alpha_S$ =0, S =0)

**Table 4.** Dynamic stability of hybrid nanocomposite plates with different layer thickness ratios and static load parameters (a/b=1, a/h=10, $V_{CN}^*$ =0.28, FG-X type, $\alpha_D/\alpha_S$=0.3, S=0)

| $\gamma$ | | $\alpha_S$ | | | | |
|---|---|---|---|---|---|---|
| | | 0 | 0.2 | 0.4 | 0.6 | 0.8 |
| 0 | $\Omega^U$ | 11.6756 | 10.6370 | 9.4853 | 8.1729 | 6.6048 |
| | $\Omega^L$ | 11.6756 | 10.2453 | 8.5798 | 6.5007 | 3.3024 |
| | $\Delta\Omega$ | 0 | 0.3917 | 0.9055 | 1.6722 | 3.3023 |
| | $\Omega_{DI}$ | 0 | 1.9435 | 4.4932 | 8.2976 | 16.3862 |
| 5 | $\Omega^U$ | 12.9034 | 11.7555 | 10.4827 | 9.0323 | 7.2992 |
| | $\Omega^L$ | 12.9034 | 11.3226 | 9.4820 | 7.1842 | 3.6494 |
| | $\Delta\Omega$ | 0 | 0.4329 | 1.0008 | 1.8481 | 3.6498 |
| | $\Omega_{DI}$ | 0 | 2.3820 | 5.5070 | 10.1698 | 20.0840 |
| 10 | $\Omega^U$ | 12.8603 | 11.7163 | 10.4478 | 9.0023 | 7.2749 |
| | $\Omega^L$ | 12.8603 | 11.2849 | 9.4504 | 7.1604 | 3.6376 |
| | $\Delta\Omega$ | 0 | 0.4314 | 0.9974 | 1.8419 | 3.6374 |
| | $\Omega_{DI}$ | 0 | 2.6233 | 6.0647 | 11.1997 | 22.1173 |
| $\infty$ | $\Omega^U$ | 10.0060 | 9.1158 | 8.1288 | 7.0041 | 5.6601 |
| | $\Omega^L$ | 10.0060 | 8.7802 | 7.3528 | 5.5709 | 2.8297 |
| | $\Delta\Omega$ | 0 | 0.3357 | 0.7761 | 1.4332 | 2.8304 |
| | $\Omega_{DI}$ | 0 | 4.9959 | 11.5501 | 21.3297 | 42.1245 |

**Table 5.** Dynamic stability of hybrid nanocomposite plates with different layer thickness ratios and dynamic load parameters (a/b=1, a/h=10, $V_{CN}^*$ =0.28, FG-X type, $\alpha_S$=0.1, S=0)

| $\gamma$ | | $\alpha_D$ | | | | |
|---|---|---|---|---|---|---|
| | | 0 | 0.4 | 0.8 | 1.2 | 1.6 |
| 0 | $\Omega^U$ | 11.0765 | 12.2455 | 13.3122 | 14.2996 | 15.2231 |
| | $\Omega^L$ | 11.0765 | 9.7685 | 8.2559 | 6.3950 | 3.6922 |
| | $\Delta\Omega$ | 0 | 2.4770 | 5.0563 | 7.9046 | 11.5309 |
| | $\Omega_{DI}$ | 0 | 12.2907 | 25.0896 | 39.2229 | 57.2166 |
| 5 | $\Omega^U$ | 12.2412 | 13.5332 | 14.7121 | 15.8034 | 16.8240 |
| | $\Omega^L$ | 12.2412 | 10.7957 | 9.1240 | 7.0674 | 4.0802 |
| | $\Delta\Omega$ | 0 | 2.7375 | 5.5881 | 8.7360 | 12.7438 |
| | $\Omega_{DI}$ | 0 | 15.0638 | 30.7503 | 48.0725 | 70.1266 |
| 10 | $\Omega^U$ | 12.2004 | 13.4880 | 14.6630 | 8.7067 | 16.7678 |
| | $\Omega^L$ | 12.2004 | 10.7597 | 9.0937 | 15.7506 | 4.0669 |
| | $\Delta\Omega$ | 0 | 2.7283 | 5.5694 | 8.7067 | 12.7009 |
| | $\Omega_{DI}$ | 0 | 16.5895 | 33.8648 | 52.9413 | 77.2285 |
| $\infty$ | $\Omega^U$ | 9.4925 | 10.4944 | 11.4086 | 12.2548 | 13.0463 |
| | $\Omega^L$ | 9.4925 | 8.3716 | 7.0752 | 5.4803 | 3.1638 |
| | $\Delta\Omega$ | 0 | 2.1228 | 4.3334 | 6.7745 | 9.8824 |
| | $\Omega_{DI}$ | 0 | 31.5940 | 64.4942 | 100.8251 | 147.0811 |

The effect of the layer thickness ratio on the excitation frequency, instability area and dynamic instability index of FG-X type hybrid nanocomposite plates under various static and dynamic load parameters are showed in Tables 4 and 5. The static load parameter varies from 0 to 0.8 and the ratio of $\alpha_D/\alpha_S$ is kept at 0.3 in Table 4. The increasing static load parameter increase both the upper and lower frequencies, respectively. However, the increase in the dynamic load parameter enlarges the upper excitation frequency but reduces the lower one. The excitation frequencies vary against the static and dynamic load parameters in a similar way as shown Figs. 3 and 4. The layer thickness ratio always increases the dynamic instability index regardless of the magnitude of the static or dynamic load parameter. A higher layer thickness ratio and load parameter result in a larger dynamic instability index. Thus, the hybrid nanocomposite plate with a larger layer thickness ratio is more dynamically unstable under higher load parameters.

The effects of different CNT distribution types on the dynamic instability of hybrid nanocomposite plates under various static and dynamic load parameters are presented in Tables 6 and 7, respectively. It can be seen that the FG-X type CNT distribution profile causes a larger instability region, but produces a smaller dynamic instability index. On the other hand, the distribution of FG-O type CNTs leads to a decrease in unstable regions and an increase in the dynamic instability index. The comparison between the three CNT distribution types shows that the hybrid nanocomposite plate with FG-X core is the most dynamically stable, followed by FG-U and FG-O cores. In general, the influence of the distribution profile on the instability region and the dynamic instability index is not as significant as the static and dynamic load parameters.

**Table 6.** Dynamic stability of hybrid nanocomposite plates with different carbon nanotube distribution types and static load parameters (a/b=1, a/h=10, $V_{CN}^{*}$ =0.28, γ=10, $\alpha_D/\alpha_S$= 0.3, S=0)

| Core type | | $\alpha_S$ | | | | |
|---|---|---|---|---|---|---|
| | | 0 | 0.2 | 0.4 | 0.6 | 0.8 |
| FG-U | $\Omega^U$ | 12.4114 | 11.3073 | 10.0831 | 8.6880 | 7.0210 |
| | $\Omega^L$ | 12.4114 | 10.8910 | 9.1205 | 6.9104 | 3.5106 |
| | $\Delta\Omega$ | 0 | 0.4164 | 0.9626 | 1.7776 | 3.5104 |
| | $\Omega_{DI}$ | 0 | 2.8226 | 6.5256 | 12.0507 | 23.7979 |
| FG-O | $\Omega^U$ | 11.9190 | 10.8587 | 9.6831 | 8.3434 | 6.7425 |
| | $\Omega^L$ | 11.9190 | 10.4589 | 8.7587 | 6.6364 | 3.3716 |
| | $\Delta\Omega$ | 0 | 0.3998 | 0.9244 | 1.7070 | 3.3710 |
| | $\Omega_{DI}$ | 0 | 3.0672 | 7.0911 | 13.0949 | 25.8594 |
| FG-X | $\Omega^U$ | 12.8603 | 11.7163 | 10.4478 | 9.0023 | 7.2749 |
| | $\Omega^L$ | 12.8603 | 11.2849 | 9.4504 | 7.1604 | 3.6376 |
| | $\Delta\Omega$ | 0 | 0.4314 | 0.9974 | 1.8419 | 3.6374 |
| | $\Omega_{DI}$ | 0 | 2.6233 | 6.0647 | 11.1997 | 22.1173 |

**Table 7.** Dynamic stability of hybrid nanocomposite plates with different carbon nanotube distribution types and dynamic load parameters (a/b=1, a/h=10, $V_{CN}^{*}$ =0.28, $\gamma$ =10, $\alpha_s$ =0.1, S=0).

| Core type | | $\alpha_D$ | | | | |
|---|---|---|---|---|---|---|
| | | 0 | 0.4 | 0.8 | 1.2 | 1.6 |
| FG-U | $\Omega^U$ | 11.7745 | 13.0172 | 14.1512 | 15.2008 | 16.1825 |
| | $\Omega^L$ | 11.7745 | 10.3841 | 8.7762 | 6.7980 | 3.9249 |
| | $\Delta\Omega$ | 0 | 2.6331 | 5.3750 | 8.4027 | 12.2576 |
| | $\Omega_{DI}$ | 0 | 17.8500 | 36.4381 | 56.9641 | 83.0968 |
| FG-O | $\Omega^U$ | 11.3074 | 12.5007 | 13.5897 | 14.5977 | 15.5404 |
| | $\Omega^L$ | 11.3074 | 9.9722 | 8.4281 | 6.5284 | 3.7694 |
| | $\Delta\Omega$ | 0 | 2.5285 | 5.1616 | 8.0692 | 11.7710 |
| | $\Omega_{DI}$ | 0 | 19.3969 | 39.5958 | 61.9005 | 90.2972 |
| FG-X | $\Omega^U$ | 12.2004 | 13.4880 | 14.6630 | 8.7067 | 16.7678 |
| | $\Omega^L$ | 12.2004 | 10.7597 | 9.0937 | 15.7506 | 4.0669 |
| | $\Delta\Omega$ | 0 | 2.7283 | 5.5694 | 8.7067 | 12.7009 |
| | $\Omega_{DI}$ | 0 | 16.5895 | 33.8648 | 52.9413 | 77.2285 |

**Table 8.** Dynamic stability of hybrid nanocomposite plates with different carbon nanotube volume fractions and static load parameters (a/b=1, a/h=10, FG-X type, γ=10, $\alpha_D/\alpha_S$=0.3, S=0)

| $V_{CN}^{*}$ | | $\alpha_S$ | | | | |
|---|---|---|---|---|---|---|
| | | 0 | 0.2 | 0.4 | 0.6 | 0.8 |
| 0 | $\Omega^U$ | 9.4340 | 8.5948 | 7.6643 | 6.6039 | 5.3368 |
| | $\Omega^L$ | 9.4340 | 8.2783 | 6.9326 | 5.2528 | 2.6687 |
| | $\Delta\Omega$ | 0 | 0.3165 | 0.7316 | 1.3511 | 2.6681 |
| | $\Omega_{DI}$ | 0 | 4.8177 | 11.1381 | 20.5683 | 40.6173 |
| 0.11 | $\Omega^U$ | 11.0482 | 10.0654 | 8.9756 | 7.7338 | 6.2499 |
| | $\Omega^L$ | 11.0482 | 9.6948 | 8.1188 | 6.1515 | 3.1253 |
| | $\Delta\Omega$ | 0 | 0.3706 | 0.8568 | 1.5823 | 3.1247 |
| | $\Omega_{DI}$ | 0 | 3.5293 | 8.1594 | 15.0677 | 29.7551 |
| 0.14 | $\Omega^U$ | 11.4129 | 10.3976 | 9.2719 | 7.9890 | 6.4562 |
| | $\Omega^L$ | 11.4129 | 10.0148 | 8.3867 | 6.3545 | 3.2283 |
| | $\Delta\Omega$ | 0 | 0.3829 | 0.8851 | 1.6346 | 3.2279 |
| | $\Omega_{DI}$ | 0 | 3.3116 | 7.6561 | 14.1383 | 27.9202 |
| 0.28 | $\Omega^U$ | 12.8603 | 11.7163 | 10.4478 | 9.0023 | 7.2749 |
| | $\Omega^L$ | 12.8603 | 11.2849 | 9.4504 | 7.1604 | 3.6376 |
| | $\Delta\Omega$ | 0 | 0.4314 | 0.9974 | 1.8419 | 3.6374 |
| | $\Omega_{DI}$ | 0 | 2.6233 | 6.0647 | 11.1997 | 22.1173 |

Tables 8 and 9 present the effects of various CNT volume fractions on the dynamic instability of FG-X type hybrid nanocomposite plates subjected to the static and dynamic load parameters. Tables 8 and 9 indicate that the plate stiffness increases with the increase of the CNT volume fraction, which results in a larger instability region, but the dynamic instability index is reduced to improve stability. Therefore, the increasing CNT volume fraction has a tendency to enhance the dynamic stability of the hybrid nanocomposite plate. Figures 5 and 6 show the effects of static load parameter on the instability region and

dynamic instability index for the FG-X type hybrid nanocomposite plates with various CNTs volume fractions. It can be seen that the increasing static load $|\alpha_S|$ increases the instability region and dynamic instability index regardless of the CNT volume fraction. However, with the increase in CNT volume fraction, the instability region is enlarged but the dynamic instability index is reduced. Additionally, the compressive static load ($\alpha_S > 0$) has a more significant effect on the unstable region and dynamic instability index than the tensile static load has.

**Table 9.** Dynamic stability of hybrid nanocomposite plates with different carbon nanotube volume fractions and dynamic load parameters (a/b=1, a/h=10, FG-X type, $\gamma$ =10, $\alpha_S$ =0.1, S=0)

| $V_{CN}^*$ | | $\alpha_D$ | | | | |
|---|---|---|---|---|---|---|
| | | 0 | 0.4 | 0.8 | 1.2 | 1.6 |
| 0 | $\Omega^U$ | 8.9499 | 9.8944 | 10.7564 | 11.5542 | 12.3004 |
| | $\Omega^L$ | 8.9499 | 7.8931 | 6.6709 | 5.1674 | 2.9836 |
| | $\Delta\Omega$ | 0 | 2.0014 | 4.0855 | 6.3868 | 9.3167 |
| | $\Omega_{DI}$ | 0 | 30.4672 | 62.1939 | 97.2283 | 141.8312 |
| 0.11 | $\Omega^U$ | 10.4812 | 11.5874 | 12.5968 | 13.5312 | 14.4050 |
| | $\Omega^L$ | 10.4812 | 9.2436 | 7.8123 | 6.0515 | 3.4941 |
| | $\Delta\Omega$ | 0 | 2.3438 | 4.7845 | 7.4797 | 10.9110 |
| | $\Omega_{DI}$ | 0 | 22.3192 | 45.5611 | 71.2262 | 103.9009 |
| | $\Omega^U$ | 10.8272 | 11.9699 | 13.0126 | 13.9778 | 14.8805 |
| 0.14 | $\Omega^L$ | 10.8272 | 9.5487 | 8.0702 | 6.2512 | 3.6093 |
| | $\Delta\Omega$ | 0 | 2.4212 | 4.9425 | 7.7266 | 11.2712 |
| | $\Omega_{DI}$ | 0 | 20.9424 | 42.7507 | 66.8326 | 97.4922 |
| 0.28 | $\Omega^U$ | 12.2004 | 13.4880 | 14.6630 | 8.7067 | 16.7678 |
| | $\Omega^L$ | 12.2004 | 10.7597 | 9.0937 | 15.7506 | 4.0669 |
| | $\Delta\Omega$ | 0 | 2.7283 | 5.5694 | 8.7067 | 12.7009 |
| | $\Omega_{DI}$ | 0 | 16.5895 | 33.8648 | 52.9413 | 77.2285 |

**Table 10.** Dynamic stability of hybrid nanocomposite plates with different bending stress parameters and compressive loads (a/b=1, a/h=10, FG-X type, $V_{CN}^*$ =0.28, $\gamma$=10, $\alpha_D/\alpha_S$=0.3)

| $\alpha_S$ | | S | | | | |
|---|---|---|---|---|---|---|
| | | 0 | 5 | 10 | 15 | 20 |
| 0.2 | $\Omega^U$ | 11.7163 | 11.7154 | 11.7125 | 11.7077 | 11.7010 |
| | $\Omega^L$ | 11.2849 | 11.2831 | 11.2776 | 11.2685 | 11.2558 |
| | $\Delta\Omega$ | 0.4314 | 0.4323 | 0.4349 | 0.4392 | 0.4452 |
| | $\Omega_{DI}$ | 2.6233 | 2.6285 | 2.6442 | 2.6705 | 2.7073 |
| 0.4 | $\Omega^U$ | 10.4478 | 10.4435 | 10.4306 | 10.4091 | 10.3788 |
| | $\Omega^L$ | 9.4504 | 9.4417 | 9.4156 | 9.3718 | 9.3098 |
| | $\Delta\Omega$ | 0.9974 | 1.0018 | 1.0150 | 1.0373 | 1.0690 |
| | $\Omega_{DI}$ | 6.0647 | 6.0914 | 6.1719 | 6.3074 | 6.5001 |
| 0.8 | $\Omega^U$ | 7.2749 | 7.2503 | 7.1755 | 7.0483 | 6.8642 |
| | $\Omega^L$ | 3.6376 | 3.5463 | 3.2551 | 2.6929 | 1.5747 |
| | $\Delta\Omega$ | 3.6374 | 3.7040 | 3.9205 | 4.3554 | 5.2895 |
| | $\Omega_{DI}$ | 22.1173 | 22.5226 | 23.8387 | 26.4830 | 32.1633 |

**Table 11.** Dynamic stability of hybrid nanocomposite plates with different bending stress parameters and tensile loads (a/b=1, a/h=10, FG-X type, $V_{CN}^*$ =0.28, $\gamma$=10, $\alpha_D/|\alpha_S|$=0.3).

| $\alpha_S$ | | S | | | | |
|---|---|---|---|---|---|---|
| | | 0 | 5 | 10 | 15 | 20 |
| -0.2 | $\Omega^U$ | 14.2628 | 14.2613 | 14.2570 | 14.2498 | 14.2397 |
| | $\Omega^L$ | 13.9106 | 13.9098 | 13.9073 | 13.9033 | 13.8977 |
| | $\Delta\Omega$ | 0.3522 | 0.3516 | 0.3497 | 0.3465 | 0.3421 |
| | $\Omega_{DI}$ | 2.1417 | 2.1378 | 2.1263 | 2.1070 | 2.0800 |
| -0.4 | $\Omega^U$ | 15.5392 | 15.5339 | 15.5180 | 15.4915 | 15.4540 |
| | $\Omega^L$ | 14.8869 | 14.8839 | 14.8748 | 14.8597 | 14.8385 |
| | $\Delta\Omega$ | 0.6523 | 0.6500 | 0.6432 | 0.6317 | 0.6155 |
| | $\Omega_{DI}$ | 3.9662 | 3.9524 | 3.9109 | 3.8411 | 3.7424 |
| -0.8 | $\Omega^U$ | 17.8198 | 17.8013 | 17.7455 | 17.6509 | 17.5149 |
| | $\Omega^L$ | 16.6689 | 16.6581 | 16.6257 | 16.5711 | 16.4935 |
| | $\Delta\Omega$ | 1.1509 | 1.1432 | 1.1198 | 1.0798 | 1.0214 |
| | $\Omega_{DI}$ | 6.9981 | 6.9513 | 6.8092 | 6.5657 | 6.2105 |

Figures 7 and 8 present the variations of the instability region and dynamic instability index against the dynamic load parameters for the FG-X type hybrid nanocomposite plates under various static loads. The results show that the instability region and dynamic instability index increase with the dynamic load. The instability region and dynamic instability index increase with the compressive static load ($\alpha_S > 0$), but decrease as the tensile static load ($\alpha_S < 0$) increases. Therefore, increasing the static compression load has the effect of making the hybrid nanocomposite plate more unstable under higher dynamic loads. However, the compressive static load produces a more significant influence on the instability region and dynamic instability index than the tensile one. It is also found that compressive static load will significantly increase the dynamic instability of the hybrid nanocomposite plate when it is subjected to a higher dynamic load.
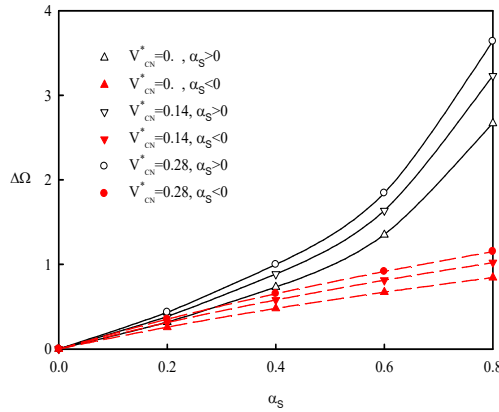


**Fig. 5.** Effect of static load parameters on the instability region for different carbon nanotube volume fractions (a/b=1, a/h=10, FG-X type, $\gamma$=10, $\alpha_D/|\alpha_S|$=0.3, S=0)
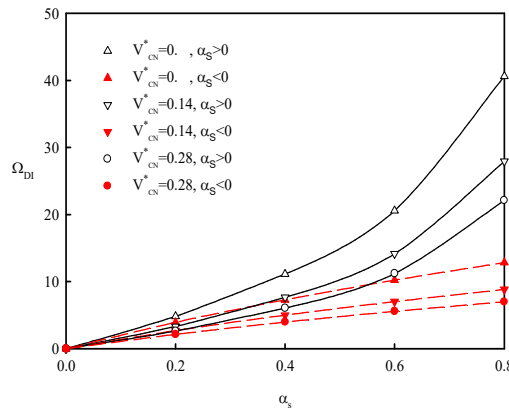


**Fig. 6.** Effect of static load parameters on the dynamic instability index for different carbon nanotube volume fractions (a/b=1, a/h=10, FG-X type, $\gamma$=10, $\alpha_D/|\alpha_S|$=0.3, S=0)



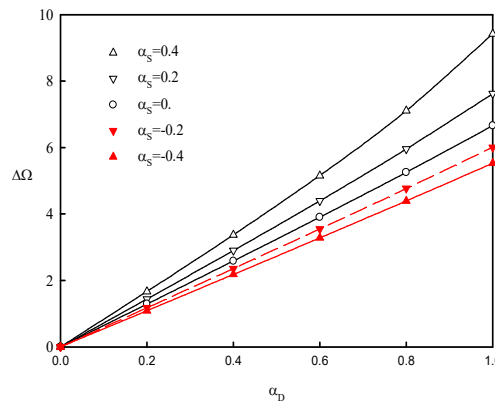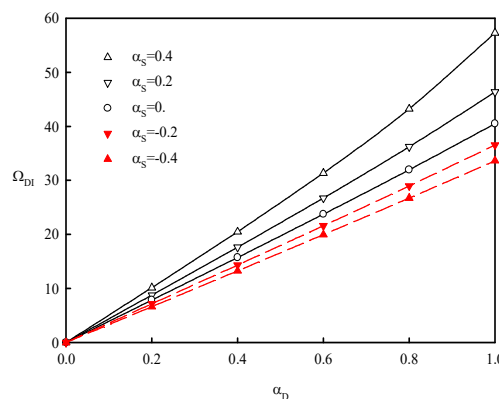**Fig. 7.** Effect of dynamic load parameters on the instability region for various static load parameters (a/b=1, a/h=10, $V_{CN}^*$ =0.28, FG-X type, $\gamma$=10, S=0)

**Table 12.** Dynamic stability of hybrid nanocomposite plates under different bending stress parameters and dynamic loads. (a/b=1, a/h=10, FG-X type, $V_{CN}^*$ =0.28, $\gamma$=10, $\alpha_S$=0.1)

| $\alpha_D$ | | S | | | | |
|---|---|---|---|---|---|---|
| | | 0 | 5 | 10 | 15 | 20 |
| 0.4 | $\Omega^U$ | 13.4880 | 13.4877 | 13.4869 | 13.4854 | 13.4834 |
| | $\Omega^L$ | 10.7597 | 10.7565 | 10.7468 | 10.7305 | 10.7077 |
| | $\Delta\Omega$ | 2.7283 | 2.7312 | 2.7401 | 2.7549 | 2.7758 |
| | $\Omega_{DI}$ | 16.5895 | 16.6074 | 16.6614 | 16.7515 | 16.8782 |
| 0.8 | $\Omega^U$ | 14.6630 | 14.6606 | 14.6535 | 14.6416 | 14.6248 |
| | $\Omega^L$ | 9.0937 | 9.0830 | 9.0509 | 8.9970 | 8.9205 |
| | $\Delta\Omega$ | 5.5694 | 5.5776 | 5.6026 | 5.6446 | 5.7044 |
| | $\Omega_{DI}$ | 33.8648 | 33.9151 | 34.0668 | 34.3223 | 34.6857 |
| 1.6 | $\Omega^U$ | 16.7678 | 16.7565 | 16.7223 | 16.6647 | 16.5829 |
| | $\Omega^L$ | 4.0669 | 3.9890 | 3.7439 | 3.2894 | 2.5022 |
| | $\Delta\Omega$ | 12.7009 | 12.7675 | 12.9783 | 13.3753 | 14.0806 |
| | $\Omega_{DI}$ | 77.2285 | 77.6333 | 78.9153 | 81.3291 | 85.6180 |



**Fig. 8.** Effect of dynamic load parameters on the dynamic instability index for various static load parameters (a/b=1, a/h=10, $V_{CN}^*$ =0.28, FG-X type, $\gamma$=10, S=0)

Tables 10 and 11 show the effects of bending stress parameters on the dynamic stability of FG-X hybrid nanocomposite plates under various compressive and tensile loads, respectively. The bending stress increases the instability region and dynamic instability index for hybrid nanocomposite plates under compressive loads, but the effect of bending stress is reversed for those under tensile loads. Moreover, the effect of bending stress is more significant at higher compressive loads, but it is less obvious at lower compressive loads and tensile loads. Table 12 indicates the effects of bending stresses on the dynamic instability of FG-X hybrid nanocomposite plates subjected to dynamic loads. The results are similar to those in Table 10 for hybrid nanocomposite plates under compressive loads. The bending stress increases the instability region and dynamic instability index, and its effect is considerable at higher dynamic loads.

## 5. Concluding remarks

The dynamic behaviors of hybrid nanocomposite plates subjected to an arbitrary periodic load are examined and discussed. The preliminary results are summarized as follows:

1. The excitation frequency, unstable region and dynamic instability index are significantly affected by the layer thickness ratio, CNT volume fraction, static and dynamic load parameters.
2. The excitation frequency increases with the increase of the layer thickness ratio, CNT volume fraction, tensile static load and dynamic load, but decreases as the compressive load and bending stress increase. The layer thickness ratio, CNT volume fraction, bending stress, static and dynamic load parameter enlarge the unstable region.
3. The dynamic instability index increases with the increase in the layer thickness, bending stress, static and dynamic loading, and reduces as the CNT volume fraction increases.

## Author Contributions

Chun-Sheng Chen planned the scheme, initiated the project, and developed the theoretical model; Chin-Ping Fung analyzed the numerical results; Hai Wang examined the theory validation. Wei-Ren Chen checked the formulation and the calculated results. The manuscript was written through the contribution of all authors. All authors discussed the results, reviewed, and approved the final version of the manuscript.

## Conflict of Interest

The authors declared no potential conflicts of interest concerning the research, authorship, and publication of this article.

# Funding

# Data Availability Statements

The datasets generated and/or analyzed during the current study are available from the corresponding author on reasonable request.

# References

[1]   Fantuzzi, N., Tornabene, F., Viola, E., A strong formulation finite element method (SFEM) based on RBF and GDQ techniques for the static and dynamic analyses of laminated plates of arbitrary shape, *Meccanica*, 49, 2014, 2503-2542.

[2]   Tornabene. F., Fantuzzi. N., Bacciocchi M., Dynamic analysis of thick and thin elliptic shell structures made of laminated composite materials, *Composite Structures*, 133, 2015, 278-299.

[3]   Sofiyev, A.H., Kuruoglu, N., Dynamic instability of three-layered cylindrical shells containing an FGM interlayer, *Thin Walled Structures*, 93, 2015, 10-21.

[4]   Sofiyev, A.H., Influences of shear stresses on the dynamic instability of exponentially graded sandwich cylindrical shells, *Composites Part B-Engineering*, 77, 2015, 349-362.

[5]   Sofiyev, A.H., Kuruoglu, N., Parametric instability of shear deformable sandwich cylindrical shells containing an FGM core under static and time dependent periodic axial loads, *International Journal of Mechanical Sciences*, 101-102, 2015,114-123.

[6]   Sofiyev, A.H., Kuruoglu, N., Domains of dynamic instability of FGM conical shells under time dependent periodic loads, *Composite Structures*, 136, 2016,139-148.

[7]   Sofiyev, A.H., Pancar, E.B., The effect of heterogeneity on the parametric instability of axially excited orthotropic conical shells, *Thin–Walled Structures* 115, 2017, 240–246.

[8]   Sofiyev, A.H., Zerin, Z., Allahverdiev, B.P., Hui, D., Turan, F., Erdem, H., The dynamic instability of FG orthotropic conical shells within the SDT, *Steel and Composite Structures*, 25, 2017, 581-591.

[9]   Enrique, G.M., Luis, R.T., Andrés, S., Bending and free vibration analysis of functionally graded graphene vs. carbon nanotube reinforced composite plates, *Composite Structures*, 186, 2018, 123-138.

[10]  Zhao, J., Choe, K., Shuai, C., Wang, A., Wang, Q., Free vibration analysis of functionally graded carbon nanotube reinforced composite truncated conical panels with general boundary conditions, *Composite Part B: Engineering*, 160, 2019, 225-240.

[11]  Avey, M., Yusufoglu, E., On the solution of large-amplitude vibration of carbon nanotube-based double-curved shallow shells, *Mathematical Methods in the Applied Sciences*, 2020, 1–13.

[12]  Yusufoglu, E., Avey, M., Nonlinear dynamic behavior of hyperbolic paraboloidal shells reinforced by carbon nanotubes with various distributions, *Journal of Applied and Computational Mechanics*, 7, 2021, 913-921.

[13]  Sofiyev, A.H., Avey, M., Kuruoglu, N., An approach to the solution of nonlinear forced vibration problem of structural systems reinforced with advanced materials in the presence of viscous damping, *Mechanical Systems and Signal Processing*, 161, 2021, 107991.

[14]  Ansari, R., Gholami, R., Sahmani, S., On the dynamic stability of embedded single-walled carbon nanotubes including thermal environment effects, *Scientia Iranica*, 19, 2012, 919-925.

[15]  Yas, M.H., Heshmati, M., Dynamic analysis of functionally graded nanocomposite beams reinforced by randomly oriented carbon nanotube under the action of moving load, *Applied Mathematical Modelling*, 36, 2012, 1371-1394.

[16]  Bhardwaj, G., Upadhyay, A.K., Pandey R., Non-linear flexural and dynamic response of CNT reinforced laminated composite plates, *Composite Part B: Engineering*, 45, 2013, 89-100.

[17]  Rasool, M.D., Foroutan, M., Pourasghar A., Dynamic analysis of functionally graded nanocomposite cylinders reinforced by carbon nanotube by a mesh-free method, *Materials & Design*, 44, 2013, 256-266.

[18]  Ke, L.L., Yang J., Dynamic stability of functionally graded carbon nanotube-reinforced composite beams, *Mechanics of Advanced Materials and Structures*, 20, 2013, 28-37.

[19]  Rafiee, M., He, X.Q., Liew, K.M., Non-linear dynamic stability of piezoelectric functionally graded carbon nanotube-reinforced composite plates with initial geometric imperfection, *International Journal of Non-Linear Mechanics*, 59, 2014, 37-51.

[20]  Lei, Z.X., Zhang, L.W. and Liew, K.M., Dynamic stability analysis of carbon nanotube-reinforced functionally graded cylindrical panels using the element-free kp-Ritz method, *Composite Structures*, 113, 2014, 328-338.

[21]  Lei, Z.X., Zhang. L.W., Liew, K.M., Elastodynamic analysis of carbon nanotube-reinforced functionally graded plates, *International Journal of Mechanic Science*, 99, 2015, 208-217.

[22]  Belkorissat, I., Houari, M.S.A., Tounsi, A., On vibration properties of functionally graded nano-plate using a new nonlocal refined four variable model, *Steel and Composite Structures*, 18, 2015, 1063-1081.

[23]  Wang, Z.X, Shen, H.S., Nonlinear dynamic response of nanotube-reinforced composite plates resting on elastic foundations in thermal environments, *Nonlinear Dynamics*, 70, 2012, 735-754.

[24]  Sayer, M., Bektas, N.B., Sayman, B., An experimental investigation on the impact behavior of hybrid composite plates, *Composite Structures*, 92, 2010, 1256-1262.

[25]  Fu Y., Zhong J., Shao X., Tao C., Analysis of nonlinear dynamic stability for carbon nanotube-reinforced composite plates resting on elastic foundations, *Mechanics of Advances Materials Structures*, 23, 2016, 1284-1289.

[26]  Wu H., Yang J., Kitipornchai S., Parametric instability of thermo-mechanically loaded functionally graded graphene reinforced nanocomposite plates, *International Journal of Mechanic Science*, 135, 2018, 431-440.

[27]  Singh V., Kumar R., Patel S.N., Parametric instability analysis of functionally graded CNT-reinforced composite (FG-CNTRC) plate subjected to different types of non-uniform in-plane loading, In: Singh S.B., Sivasubramanian M.V.R., Chawla H. (eds) *Emerging Trends of Advanced Composite Materials in Structural Applications. Composites Science and Technology*. Springer, Singapore, 2021.

[28]  Kapuria, S., Yasin, M.Y., Active vibration suppression of multilayered plates integrated with piezoelectric fiber reinforced composites using an efficient finite element model, *Journal of Sound and Vibration*, 329, 2010, 3247-3265.

[29]  Khalili, S.M.R., Dehkordi, M.B., Carrera, E., Non-linear dynamic analysis of a sandwich beam with pseudoelastic SMA hybrid composite faces based on higher order finite element theory, *Composite Structures*, 96, 2013, 243-255.

[30]  Frikh, A., Zghal, S., Dammak, F., Dynamic analysis of functionally graded carbon nanotubes-reinforced plate and shell structures using a double directors finite shell element, *Aerospace Science and Technology*, 78, 2018, 438-451.

[31]  Harras, B., Benamar, R., Whit, R.G., Experimental and theoretical investigation of the linear and non-linear dynamic behaviour of a glare 3 hybrid composite panel, *Journal of Sound and Vibration*, 252, 2002, 281-315.

[32]  Kao, J.Y., Chen, C.S., Chen, W.R., Parametric vibration response of foam-filled sandwich plates under pulsating loads, *Mechanics of Composite Materials*, 48, 2012, 525-538.

[33]  Chen, C.S., Liu, F.H., Chen, W.R., Dynamic characteristics of functionally graded material sandwich plate in thermal environments, *Mechanics of Advanced Materials and Structures*, 24, 2017, 157-167.

[34]  Chen, C.S., Fung, C.P., Yang, J.G., Assessment of plate theories for initially stressed hybrid laminated plates, *Composite Structures*, 88, 2009, 195-201.

[35]  Chen, L.W., Yang, J.Y., Dynamic stability of laminated composite plates by the finite element method, *Computer and Structures*, 36, 1990, 845-851.

[36]  Chattopadhyay, A., Radu, A.G., Dragomir-Daescu D., A higher order plate theory for dynamic stability analysis of delaminated composite plates, *Computational Mechanics*, 26, 2000, 302-308.

[37]  Shen, H.S., Nonlinear bending of functionally graded carbon nanotube reinforced composite plates in thermal environments, *Composite*

*Structures*, 91, 2009, 9-19.

[38]  Zhang, C.L., Shen, H.S., Temperature dependent elastic properties of single-walled carbon nanotubes: prediction from molecular dynamics simulation, *Applied Physics Letters*, 89, 2006, 81904-81907.

[39]  Shen, H.S., Zhang, C.L. Thermal buckling and postbuckling behavior of functionally graded carbon nanotube-reinforced composite plates, *Materials & Design*, 31, 2010, 3403-3411.

[40]  Wang, Z.X., Shen, H.S., Nonlinear vibration of nanotube-reinforced composite plates in thermal environments, *Computational Materials Science*, 50, 2011, 2319-2330.

[41]  Alibeigloo, A., Emtehani, A., Static and free vibration analyses of carbon nanotube-reinforced composite plate using differential quadrature method, *Meccanica*, 50, 2015, 61-76.

[42]  Lei, Z.X., Liew, K.M., Yu, J.L., Buckling analysis of functionally graded carbon nanotube-reinforced composite plates using the element-free kp-Ritz method, *Composite Structures*, 98, 2013, 160-168.

[43]  Malekzadeh, P., Shojaee, M., Buckling analysis of quadrilateral laminated plates with carbon nanotubes reinforced composite layers, *Thin-Walled Structures*, 71, 2013, 108–118.

## ORCID iD

Chun-Sheng Chen  https://orcid.org/0000-0002-8343-4757

Chin-Ping Fung  https://orcid.org/0000-0002-8948-4835

Hai Wang  https://orcid.org/0000-0003-2390-4152

Wei-Ren Chen  https://orcid.org/0000-0002-4655-8769

**Publisher's Note** Shahid Chamran University of Ahvaz remains neutral with regard to jurisdictional claims in published maps and institutional affiliations.